Kufa Journal of Engineering
Vol. 17, No. 1, January 2026, P.P. 380-399
Article history: Received 19 March 2025, last revised 29 April 2025, accepted 12 May 2025

EXPERIMENTAL INVESTIGATION OF FLEXURAL PERFORMANCE OF T-SHAPED HYBRID CONCRETE BEAMS RETROFITTED WITH NSM TECHNIQUE USING GFRP BARS

Meqdam Y. Y. Al-Jabban[1] and Haider A. A. Al-Katib[2]

[1] MSc. Student, Department of Civil Engineering, Engineering Faculty, University of Kufa, Najaf, Iraq. Email: meqdamaljabban@gmail.com

[2] Prof. Dr., Department of Civil Engineering, Engineering Faculty, University of Kufa, Najaf, Iraq. Email: hayder.alkatib@uokufa.edu.iq

https://doi.org/10.30572/2018/KJE/170121

ABSTRACT

In this research, thirteen T-shaped hybrid concrete beams were designed to investigate their flexural behavior. Flanges of all beams were cast by 106 N/mm^2 f_{cu} of self-compacting high-strength concrete (SC-HSC), while the webs were made by 45 N/mm^2 f_{cu} of normal-strength concrete (NSC). One beam was loaded up to failure as a control beam (CB), and the other beams were divided into two groups; the first group consisted of six beams preloaded by 45% of CB's ultimate load (P_u), and the other group of beams subjected to 85% of CB's P_u. Beams were retrofitted along the entire clear span using various numbers and placements of glass fiber-reinforced polymer (GFRP) bars mounted near the bottoms and side(s) surfaces. However, tests resulted in a notable enhancement ranging from 35% to 101% of retrofitted beams. At the same time, the maximum deflections of both groups witnessed a range from 21.9 mm to 34.9 mm beside CB's ultimate deflection (33.8 mm); in addition, ductility ratio, toughness, and stiffness values varied between (55.89% and 73.8% reduction), (15.95% decrement and 31.96% increment), and (2.36% and 47.83% reduction), respectively. Furthermore, the failure mode was mainly GFRP-Epoxy debonding.

KEYWORDS

Retrofitting; T-Beam; Hybrid Concrete; Self-Compacting High Strength Concrete; Flexural Behavior; Near-Surface Mounting Technique; Glass Fiber Reinforced Polymer Bars.

This work is licensed under a Creative Commons Attribution 4.0 International License.

1. INTRODUCTION

Over the past decade, structural engineering has made significant strides in performance enhancement techniques of concrete elements, including load-bearing capacity improvement, particularly elements that suffer from strength deterioration or require additional reinforcement to endure increased loads due to changing the structure's purpose or inaccurate structural design, where the near surface mounting technique using GFRP bars is considered one of the innovative and effective solutions besides the hybridization concrete types in the used structural elements. Several studies have been undertaken in this regard, such as preloaded hybrid concrete beams retrofitted by the CFRP external bonding method, which experienced an improvement in ultimate load (Al-Hilfi and Al-Katib, 2024). Another investigation of 70% Pu preloaded hybrid rectangular beams retrofitted by NSM-GFRP bars resulted in cracking load reduction and loading capacity improvement in beams with three bottom bars configuration (Joudah and Al-Katib, 2024); a slight difference (6.64% of ultimate load) was observed in one-way slabs strengthened by NSM bars that were simulated with computerized finite elements (Kamonna and Abd Al-Sada, 2021) In parallel, the EB (CFRP sheets) slightly improved ultimate load under identical pre-damaged status and retrofitting configuration, while the NSM (carbon bars) exhibited higher ductility and better debonding resistance (Aljebory and Kamonna, 2025). Moreover, T-shaped beams were fabricated of different f'c (fully of NSC), (fully of HSC), (HSC flange: NSC web), and (NSC flange: HSC web). The study indicated that the type of concrete significantly influenced the flexural behavior of strengthened concrete beams and concluded that utilizing (HSC flange: NSC web) beams increased the ultimate load and deflection while decreasing cracks occurrence compared to the (fully HSC) beam (Marzoq and Borhan, 2020). In addition, three beams were made of (fully NSC), (fully HSC), and (hybrid). Tests revealed that using hybrid concrete beams enhances ultimate load capacity and toughness and increases the deflection compared to the entire NSC beam (Al-Katib and Al-Turaihi, 2024a). Furthermore, an experiment engaged RC beams that were strengthened with Side-NSM-GFRP bars by altering bar diameters and bond lengths, which resulted in ultimate load improvement and showed that the strengthening reinforcement's bond length dramatically impacts toughness, ductility, and stiffness more than the amount of strengthening reinforcement (Hosen et al., 2017). Lightweight RC beams were strengthened by Side-NSM-GFRP bars and displayed an ultimate capacity improvement. Moreover, observation indicated that a replacement of 50% of the epoxy adhesive by a cement mortar at the mid-span almost had a similarity in ultimate capacity when 100% epoxy adhesive was used (Al Thairy and Youssef, 2023). On the other hand, a study of RC beams that were strengthened overall with the NSM-GFRP bars system

considerably increased the ultimate moment (Tang et al., 2006). Also, to imitate the work in reality, the strengthening system grooves were made between the internal faces of supporting columns, which enhanced yielding and ultimate loads (Sharaky et al., 2014). As well as differently strengthened (normal and lightweight) RC beams using NSM techniques with GFRP bars, GFRP-L steel anchors, or CFRP sheets. The findings indicated that the ultimate strength increases. The ultimate capacity and deflection of beams strengthened with combined L-steel and GFRP bars were higher than those strengthened with GFRP sheets, with debonding failure being the predominant failure mode, as "debonding is the most fundamental problem of strengthening beams using the NSM technique. The effect of this phenomenon is reduced significantly in the study using the hybrid system. However, the debonding problem still remains in force for carbon/glass-strengthened beams." (Tahmouresi et al., 2022). Furthermore, " most of the previous related research stated that the tested RC-strengthened beams with NSM FRP failed due to debonding or concrete cover separation. ". The findings demonstrated that the GFRP bars with bent ends prevented the concrete cover separation and increased loading capacity (Reda et al., 2016). Correspondingly, this study concluded that "strengthening by GFRP bar with a length equal to a clear span gives better results and prevents separation of the concrete cover since the strengthening crosses the flexural stresses region into the shear stresses region." (Al-Katib and AL-Turaihi, 2024b). Various techniques were also conducted for repairing damaged RC beams, revealing that all repaired beams exhibited substantial improvements in behavior, load capacity, stiffness, ductility, and energy absorption compared to the damaged beam. The side-NSM technique demonstrated greater energy absorption capacity and ductility than the EBR (BenSaoud et al., 2024). The adhesive material in NSM strengthening techniques was replaced by various percentages of cement mortar, which revealed the possibility of replacing less than 75% of cement mortar with the side-NSM technique when epoxy is not available; on the other side, 50% and 75% replacement of adhesive by cement mortar triggered debonding failure mode (Hosen et al., 2020). Increasing the concrete compressive strength of T-hybrid RC beam flanges increased the ultimate shear failure load (Al Shami, 2022). According to the above research, this study focuses on the flexural behavior of hybrid concrete T-shape beams using the NSM technique. These engineered beams are characterized by an amalgamation of SC-HSC in the beams' flanges with NSC webs, which gives unique structural properties that allow them to withstand substantial loads, besides showing a noticeable deflected shape, hence assuring a high safety level as an advantage. Generally, the assessed effect of utilizing the NSM technique and FRP on the flexural behavior of hybrid beams and the analysis of load exposure performance demonstrated a significant

enhancement in the behaviors, which are crucial in advancing contemporary engineering solutions, optimizing design standards, and effectively rehabilitating concrete structures.

2. METHODOLOGY

2.1. Specimens' description

Thirteen slender, simply-supported T-shaped hybrid concrete beams were engineered according to the ACI-318 Code (ACI, 2019) and symmetrically cast to investigate their flexural behaviors. The geometry of each beam is (2100 mm) in total length and (270 mm) in total height; the flange is 350 mm in width and 80 mm in thickness, made out of SC-HSC with 106 kN/mm^2 f_{cu}; the specimen's web is 150 mm in width and 190 mm height, made out of NSC of 45 kN/mm^2 f_{cu}. Specimens reinforced with (2 Ø 12 mm) primary longitudinal tension reinforcement, (4 Ø 8 mm) top reinforcement in the long direction of the flange, (9 Ø 8 @ 250 mm) A transverse reinforcement of the flange short direction, and stirrups were (2 x (8 Ø 10 mm @ 100 mm) Eight on each side, as illustrated in Fig. 1. One of the thirteen beams detailed in Table 1 had been selected as a control specimen.

Table 1. Specimens' details

Group	ID	Description	
Control	**CB**	**Beam Control subjected to load up to failure (Ultimate Load)**	
Group 1 (G1)	BR45-1B	Beam subjected to 45% of CB Ultimate Load to be retrofitted by:	1 GFRP bar at the bottom
	BR45-2B		2 GFRP bars at the bottom
	BR45-1S		1 GFRP bar on one side
	BR45-2S		2 GFRP bars, one on each side
	BR45-1B2S		3 GFRP bars, one at the bottom and one at each side
	BR45-2B1S		3 GFRP bars, two at the bottom and one on one side
Group 2 (G2)	BR85-1B	Beam subjected to 85% of CB Ultimate Load to be retrofitted by:	1 GFRP bar at the bottom
	BR85-2B		2 GFRP bars at the bottom
	BR85-1S		1 GFRP bar on one side
	BR85-2S		2 GFRP bars, one on each side
	BR85-1B2S		3 GFRP bars, one at the bottom and one at each side
	BR85-2B1S		3 GFRP bars, two at the bottom and one on one side

2.2. Materials and specimens' preparation

Several mix batches were attempted using different portions of Portland Limestone Cement until the two targeted concrete mixtures were produced; all specimen flanges were made of SC-HSC with 106 N/mm^2 f_{cu} and a web of NSC 45 N/mm^2. MegaAdd MS(D) Silica Fume was 8% of cement weight, and the Flocrete PC260 (DCP-Hyperplast) admixture was 2.7% of cementitious materials. Tables 2a, 2b, and 2c detail the concrete mixture components, fresh concrete tests, and the mechanical properties of hardened concrete. Based on the structural design and ASTM A615/A615M requirements (ASTM, 2024), three different nominal sizes (Ø 8, 10 & 12) mm of steel bars with yield strength (468, 496, and 503) N/mm^2, respectively,

were used for the specimens' reinforcement. Furthermore, a single nominal size ($\emptyset$ 12 mm) of Russian GFRP bars with mean tensile strength, modulus of elasticity, and elongation (strain %) (1331 N/mm^2, 51197 N/mm^{2,} and 2.467 %), respectively, was used in the NSM retrofitting technique that was mounted in prepared grooves, in different numbers and positions using Sikadur 30 LP epoxy resin. The steel cages were placed in the (18 mm thickness) plywood molds; furthermore, a portable 22 rpm concrete mixer was used to produce both types of concrete, and curing was for about 14 days.

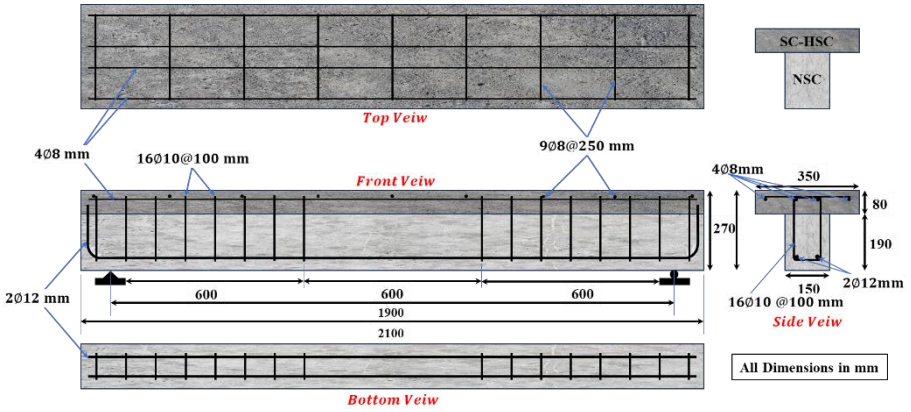

Fig. 1. Specimen dimensions and reinforcement details

Table 2a. Components details of concrete mixtures per one cubic meter

Concrete Type	C* (Kg)	S.F* (Kg)	F.A* (Kg)	C.A* (Kg)	W* (L)	SP* (L)
NSC	290	-	700	1200	160	2.5
SC-HSC	550	44	615	1100	121	15

***C**: Cement (PLC / CEM II/A-L 42.5 R), **S.F**: Silica Fume, **F.A**: Fine Aggregate (Zone 2), **C.A**: Coarse Aggregate (NSC: Partially Crashed 5-19 mm and SC-HSC: Fully Crashed 5-14 mm), **W**: Water Tap, **SP**: Superplasticizer.

Table 2b. Fresh concrete properties

Test Type	Slump Flow (mm)	T500 (sec)	J-Ring (mm)
Results	785	4	9
Standards Limits	(650 - 800)	(2 - 5)	(0 - 10)

Table 2c. Hardened concrete mechanical properties

Concrete Type	Average of Compressive Strength f_{cu} (N/mm^2)	Average of Flexural Strength f_r (N/mm^2)	Average of Tensile Strength f_t (N/mm^2)
NSC	45[1]	5.97	3
SC-HSC	106[2]	12.25	5.46

[1] An average value of testing three cubes of size 150 mm.
[2] An average value of testing three cubes of size 100 mm.

2.3. Retrofitting details

For comparison, the CB was considered without retrofitting Fig. 2a, G1 beams were initially loaded with 45% of CB's Pu and denoted by (BR45-1B, b, BR45-1S, b, BR45-2B, b, BR45-2S,

b, BR45-1B2S, b, and BR45-2B1S, b), and G2 beams preloaded with 85% denoted as (BR85-1B, b, BR85-1S, b, BR85-2B, b, BR85-2S, b, BR85-1B2S, b, and BR85-2B1S, b), and thereafter, these beams were retrofitted in successive pairs with one, two, and three GFRP bars with a change in bars' locations between bottom and side(s) and loaded until failure, designated as (BR45-1B, a, BR45-1S, a, BR45-2B, a, BR45-2S, a, BR45-1B2S, a, and BR45-2B1S, a) and (BR85-1B, a, BR85-1S, a, BR85-2B, a, BR85-2S, a, BR85-1B2S, a, and BR85-2B1S, a) for G1 and G2, respectively, Figs. 2b and 2c show the retrofitting of the NSM system. The lowercase letters b (before) or a (after) followed the specimen ID, respectively denoted for the initial loading and the post-retrofitting stage. The NSM technique was implemented by engraving longitudinal grooves into the clear concrete covers (30 mm) of the bottom and sides surfaces; each groove measures about 1800 mm in length and 18 mm in width and depth, corresponding to 1.5 times the diameter of the GFRP bar, followed ACI-440.2R (ACI, 2017). The grooving and mounting of the GFRP bars process started with marking the grooves' locations; an angle grinder/cutting machine equipped with a 180 mm marbles' cutting wheel was utilized to make a couple of longitudinal parallel cuts based on the specified depth and width of grooves; a hammer and chisel were used to remove the concrete in between; the grooves were washed by a high-pressure water jet and dried by an air blower; mixing and the application of epoxy were according to the manufacturer's instructions; half of each groove depth was roughly filled with the epoxy paste, and then the GFRP bar was gently pushed in after cleaning with a dry piece of fabric to get rid of dust, if any. Finally, the surplus epoxy was eliminated, and complete epoxy coverage of all bars was guaranteed. At last, specimens were ready for performance investigation tests after seven days of curing.

2.4. Test setup and instrumentation

All specimens in this experiment underwent flexural testing in a four-point configuration utilizing a 2000 kN testing machine. Two digital dial gauges (50 mm range—0.01 mm resolution) were installed on magnetic-base stands beneath each beam for deflection measurements; the primary gauge was positioned at the mid-span of the specimen, while the secondary gauge was located at the quarter. The load application was at a rate of 5 kN, and all test data were manually recorded. The first cracks and load values were marked in red, while subsequent cracks were marked in black or dark blue; a crack meter was utilized to measure the crack widths of less than one millimeter, and the digital vernier caliper was used for wider cracks. Fig. 3 illustrates the schematic of the four-point bending test.

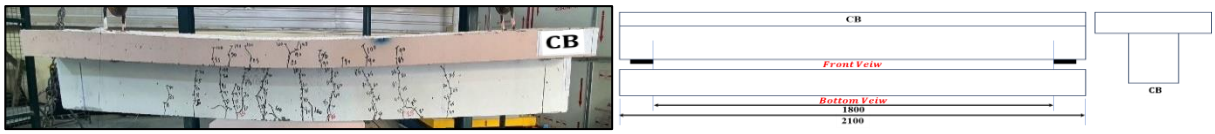

Fig. 2a. The control beam

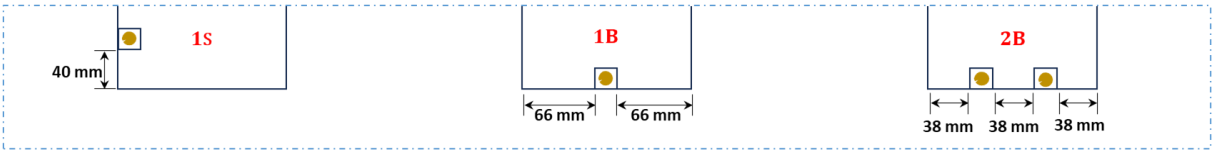

Fig. 2b. NSM technique grooves measurements.

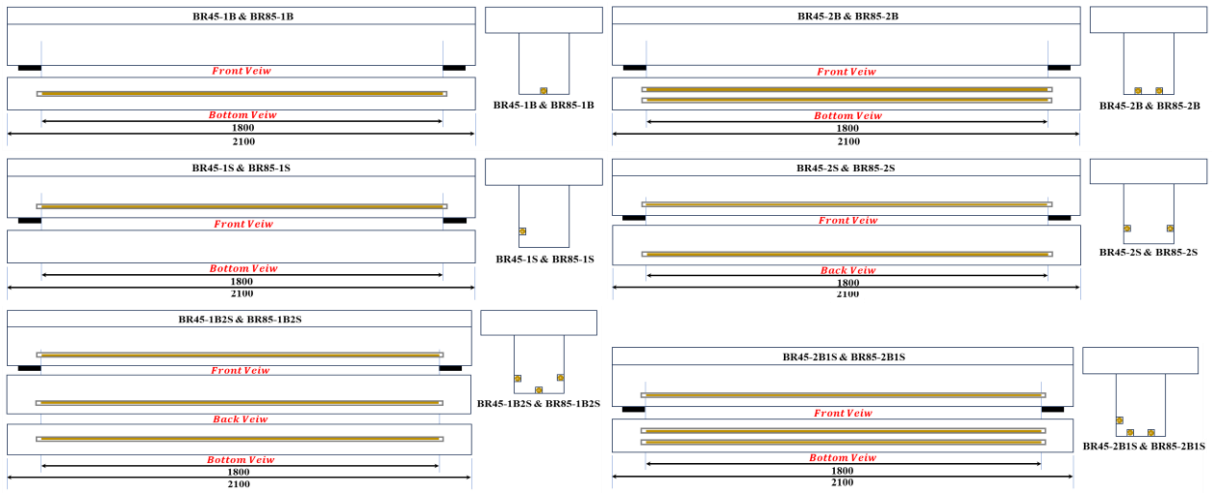

Fig. 2c. Group one and two NSM-GFRP retrofitting system

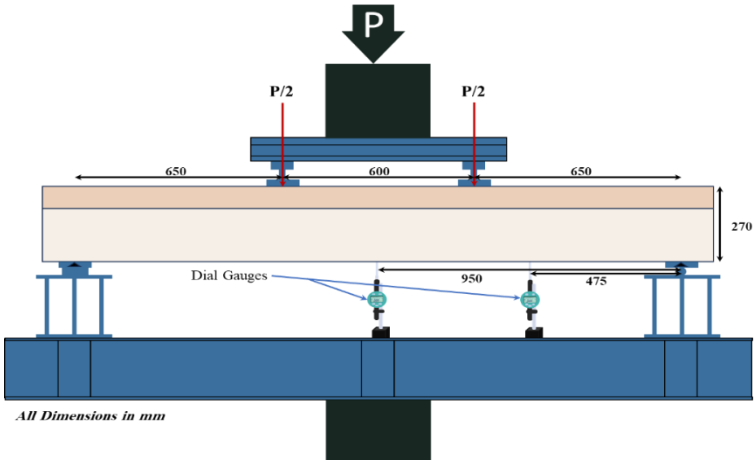

Fig. 3. Test setup

3. RESULTS AND DISCUSSION

The obtained outcomes for the CB exhibited a cracking load of 25 kN and an ultimate deflection of 33.7 mm under a maximum load capacity of 100 kN. The beams (BR45-1B, a, BR45-1S, a, BR45-2B, a, BR45-2S, a) and (BR85-1B, a, BR85-1S, a, BR85-2B, a, BR85-2S, a) demonstrated an identical decrement percentage (60%) with a cracking load (10 kN) compared to CB. At the same time, the beams (BR45-1B2S, a, and BR45-2B1S, a) behaved differently

with reduction percentages of (20% and 0%), which corresponded to cracking loads of (20 and 25 kN), respectively. In contrast, the beams (BR85-1B2S, a, and BR85-2B1S, a) showed similar behavior with a reduction of 40% and cracking loads of 15 kN. Generally, the observed reductions in the cracking load of both groups of pre-cracked beams compared to the CB cracking load might be attributed to the unintentionally of epoxy's infiltration into some pre-existing cracks and partially remediated and were prematurely fractured during the reloading process; this opinion was reinforced by the diminishing reduction percentages with the increase in the number of bars to three bars (i.e., more epoxy infiltration: more cracks remediation), particularly in the three bars hybrid configurations with two bottom bars where the cracks are more numerous and wider. The CB displayed a cracking deflection of 0.91 mm, while the other twelve beams demonstrated lesser percentages ranging from 4.4% to 41.8%, except for BR45-1B2S, a, and BR45-2B1S, a, which showed increases of 37.4% and 29.7%, respectively. Regarding the ultimate capacity and deflection of specimens considering CB values, all beams' loading capacity has significantly increased due to the retrofitting technique and recorded increments between 35% and 101%, respectively. Nevertheless, despite the beams subjected to 85% CB's Pu experienced greater damage than those preloaded with 45% CB's Pu, they exhibited relatively slight increases in ultimate loads (ranging from 7 to 16 kN) compared to those exposed to lower preloading percentages. The greater damage may seemingly have stimulated more effective activation of the retrofitting technique by an earlier involvement of GFRP bars in load resistance during the post-retrofitting stage due to an internal redistribution of stresses, particularly after exceeding the elastic limit. Conversely, the 45% preloaded beams stayed within the linear elastic range with less GFRP contribution efficiency, alongside a potential engagement of epoxy filling many deep and wide cracks that pre-existed in the most severely damaged beams, which partially restored the pre-damaged areas' strength. At the same time, most invisible microcracks in the less damaged beams remained untreated by epoxy due to their size, resulting in lower or minimal enhancement. For the maximum deflection, the twelve specimens varied between a 34.9% decrement and a 3.6% increment. The beams (BR45-1B2S, a and BR85-1B2S, a) have almost the same behavior, with the best ultimate load capacity increase (101% and 100%, respectively); furthermore, each has the third-highest mid-span deflection within its group (25.5 mm and 31.8 mm), respectively, which is very close to the deflection of CB, giving a notable alerting sign for the building's occupants; see details in Table3. Moreover, the failure mode was mainly GFRP-Epoxy debonding except for BR45-2S, a and BR85-2S, a was accompanied by concrete cover separation. In addition, ductility ratio, toughness, and stiffness values varied between (55.75% and 73.8% reduction), (15.95%

decrement and 31.96% increment), and (2.36% and 47.83% decrement), respectively, as shown in Table 4.

Table 3. Specimen's groups' results with percentage variations

Group	Specimens ID	Cracking Load (kN)	%	Cracking Deflection (mm)	%	Ultimate Load (kN)	%	Ultimate Deflection (mm)	%
Control	**CB**	25	-	0.91	-	100	-	33.7	-
G1	BR45-1B, a	10	-60	0.65	-28.6	149	49	25.4	-24.5
	BR45-2B, a	10	-60	0.60	-34.1	177	77	22.9	-31.9
	BR45-1S, a	10	-60	0.65	-28.6	140	40	30.9	-8.1
	BR45-2S, a	10	-60	0.53	-41.8	170	70	30.5	-9.4
	BR45-1B2S, a	20	-20	1.25	37.4	201	101	25.5	-24.2
	BR45-2B1S, a	25	0	1.18	29.7	192	92	21.9	-34.9
G2	BR85-1B, a	10	-60	0.57	-37.4	165	65	34.0	1.1
	BR85-2B, a	10	-60	0.63	-30.8	185	85	27.0	-19.9
	BR85-1S, a	10	-60	0.72	-20.9	135	35	30.0	-10.8
	BR85-2S, a	10	-60	0.65	-28.6	180	80	34.9	3.6
	BR85-1B2S, a	15	-40	0.84	-7.7	200	100	31.8	-5.5
	BR85-2B1S, a	15	-40	0.87	-4.4	199	99	29.1	-13.6

Table 4. Ductility, toughness, and stiffness results with percentage variations

Group	Specimens ID	Ductility Ratio	%	Toughness (kN.m)	%	Stiffness (kN/mm)	%
Control	**CB**	4.17	-	2.83	-	12.40	-
Group 1	BR45-1B, a	1.59	-61.93	2.62	-7.47	9.41	-24.09
	BR45-2B, a	1.51	-63.76	2.74	-3.35	11.79	-4.89
	BR45-1S, a	1.84	-55.89	3.19	12.83	8.37	-32.46
	BR45-2S, a	1.67	-60.06	3.72	31.25	9.32	-24.79
	BR45-1B2S, a	1.39	-66.68	3.37	18.90	11.04	-10.94
	BR45-2B1S, a	1.38	-66.96	2.76	-2.59	12.10	-2.36
Group 2	BR85-1B, a	1.31	-68.58	3.42	20.74	6.93	-44.11
	BR85-2B, a	1.14	-72.76	2.74	-3.10	8.82	-28.87
	BR85-1S, a	1.30	-68.82	2.38	-15.95	6.47	-47.83
	BR85-2S, a	1.23	-70.54	3.74	31.96	6.93	-44.07
	BR85-1B2S, a	1.16	-72.26	3.62	28.02	8.06	-34.95
	BR85-2B1S, a	1.09	-73.80	3.16	11.72	8.40	-32.23

The load-deflection curve of CB in Fig. 4a started with a vertical linear segment, which indicated the elastic response that reflected the beam stiffness and the ability to resist deformation under low to moderate loads. With the load increase, the behavior moved to nonlinearity, and deflection increased, which referred to transitioning to plastic deformation that marked a decrease in stiffness due to the yielding phase. Hence, the maximum load sustaining the beam was 100 kN, corresponding to 33.8 mm of ultimate deflection. In the end, the curve flattened and showed behavior where the beam experienced a progressive deflection under a nearly steady load; this indicates a ductile failure mechanism. In addition, the CB

remaining deflection value after loading release was 23.73 mm. Fig. 4 b also shows the control beam's yield point deflection.

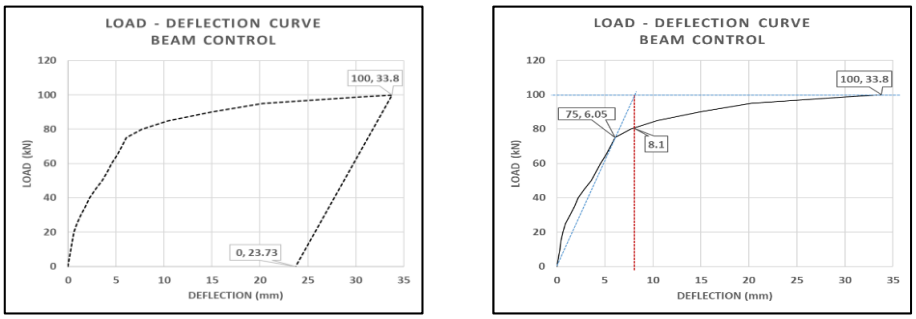

Fig. 4. (a) Load-deflection curve and (b) Yield-point of CB

Group One load-deflection curves in Figs. 5a & 5c described the structural behavior of beams retrofitted with various configurations compared to the CB that provided the benchmark for evaluating the performance optimization in the retrofitted specimens; however, the retrofitted beams showed significantly enhanced load-carrying capacities. Where the specimens (BR45-1B, a) and (BR45-2B, a) reflected an average enhancement in strength and reached (149 kN and 177 kN) as an ultimate load with deflections (25.42 mm and 22.92 mm, respectively), the specimen (BR45-2B1S, a) showed (192 kN) as its maximum load with a deflection of (21.93) mm that exhibited a significant increase in strength and stiffness. The specimen (BR45-1B2S, a) notably achieved the highest load-bearing capacity of 201 kN with a deflection of 25.53 mm, indicating the effectiveness of this retrofitting arrangement (numbers and locations of GFRP bars). The curves diagram disclosed that retrofitting techniques significantly increased the stiffness and loading capacity, while ductility altered depending on the retrofitting percentage and arrangement. Beams with more bars tend to show reduced deflections at ultimate load, which reflects a stiffer and less ductile behavior. Figs. 5b & 5d represent the load-crack width relationships for group one together with CB, where the initial behavior of all specimens exhibited a linear load increase with minimal crack width, which indicated an elastic mode and then moved to nonlinearity sets due to cracks' propagation; however, the specimens' actions varied and showed the influence of retrofitting arrangements on the performance, where all beams demonstrated narrower cracks with higher load capacity compared to CB. The beam (BR45-1B, a) displayed the highest crack width (3.53 mm) among the group beams at a load capacity equal to 149 kN, following a steady decline in load resistance as the crack widened further. The specimen (BR45-1B2S, a) showed a moderate crack width (1.18 mm) compared to the other specimens of its group. At the same time, the behaviors of specimens (BR45-2B1S, a) and (BR45-2B, a) were also marginally similar, where they showed the lowest crack widths (0.47 mm and 0.83 mm), respectively.

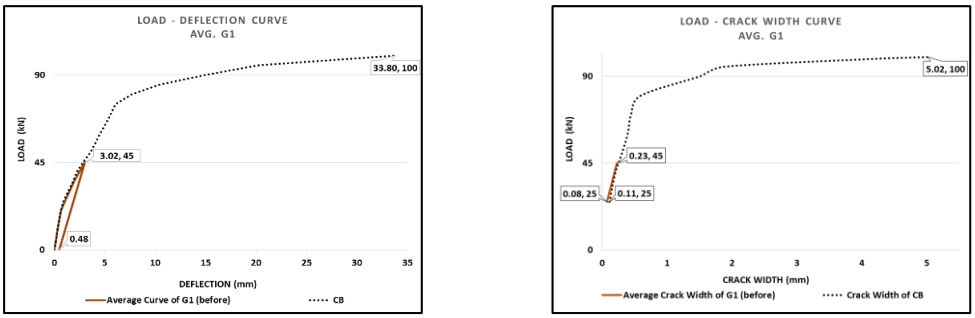

Fig. 5. (a) Avg. Load-deflection curves and (b) Avg. Load-crack width curves of G1 before retrofitting

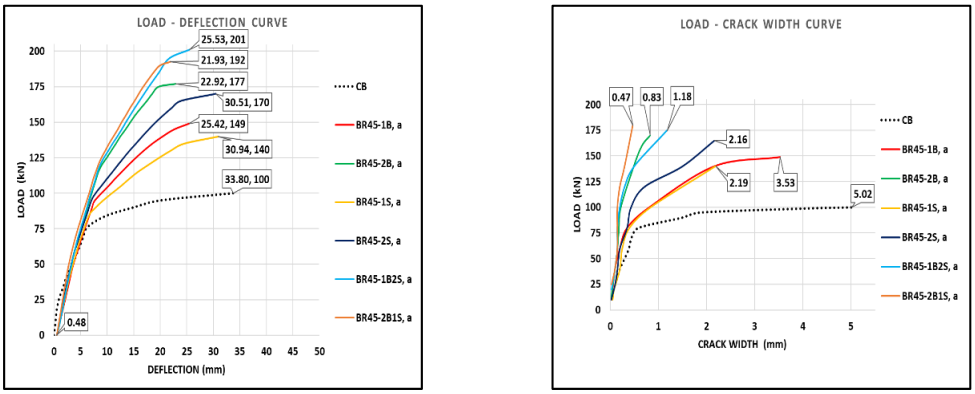

Fig. 5. (c) Load-deflection curves and (d) Load-crack width curves of G1 after retrofitting

Group Two load-deflection curves in Figs. 6a & 6c delineated the structural behavior of retrofitted beams with identical configurations to group one specimens compared to CB, where significant enhancements were observed in the retrofitted beams' load-carrying capacities and ductility mechanisms. Furthermore, the initial part of each curve displayed a linear elastic behavior, and with an increment of deflection, the nonlinearity emerged that corresponded to the initiation and propagation of cracks. The specimen (BR85-1B2S, a) achieved the highest load-bearing capacity (200 kN) at (31.83 mm) a mid-span deflection. Specimen (BR85-2B1S, a) was closely following, with an ultimate load (199 kN) at (29.11 mm) deflection. On the other hand, the specimen (BR85-1S, a) displayed the lowest ultimate load (135 kN) and (30.04 mm) mid-span deflection. The results highlight retrofitting arrangements' effect on flexural behavior, where the retrofitted beams (BR85-1B2S, a) and (BR85-2B1S, a) significantly enhanced load-bearing capacity and ductility, and emphasize the importance of tailored retrofitting techniques for optimal structural performance under flexural loads. Figs. 6b & 6d illustrate the load-crack width relationships for group two jointly with the CB, where specimens demonstrated equivalent initial linearity and nonlinearity behaviors to group one; however, all beams showed slimmer cracks with higher load capacity than CB, which were identical to the case of group one as well. The (BR85-1B2S, a) specimen indicated the highest ultimate load (200 kN) with a crack width (1.26 mm), followed by the specimen (BR85-2B1S, a) with a 199 kN ultimate load and a 1.13 mm crack width. In addition, specimen (BR85-1S, a) had the minimal load capacity

among the group specimens with a moderate crack width (1.28 mm), and (BR85-1B, a) exhibited a large crack width (3.7 mm) at moderate ultimate capacity (165 kN). These results highlighted the implications of the retrofitting technique and its bars' arrangements to significantly enhance beam performance by resisting crack propagation and maintaining load-carrying capacity, making them more reliable for practical applications.

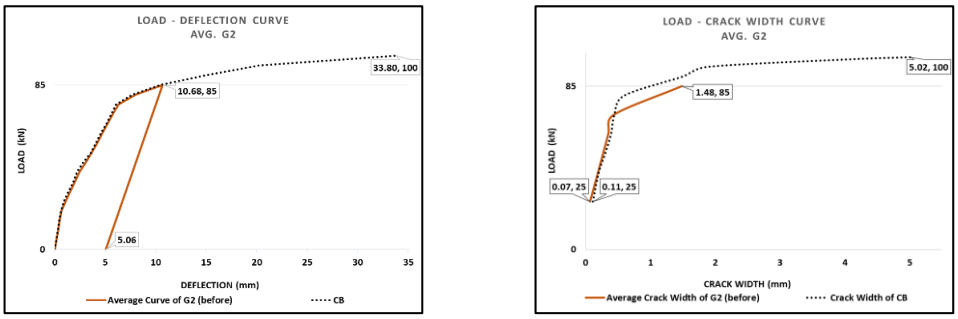

Fig. 6. (a) Avg. Load-deflection curves and
(b) Avg. Load-crack width curves of G2 before retrofitting

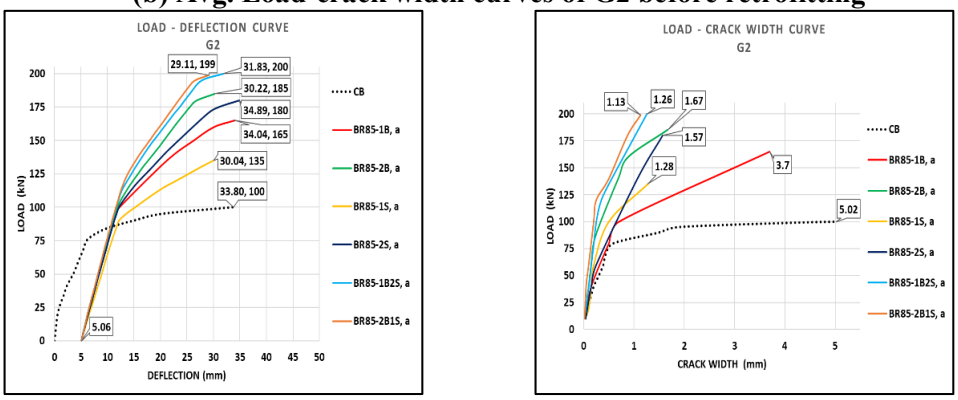

Fig. 6. (c) Load-deflection curves and (d) Load-crack width curves of G2 after retrofitting

The cracking pattern of group one Fig. 7 demonstrated a localized and less uniform cracking distribution; (BR45-1B, a), (BR45-1S, a), (BR45-2B, a), and (BR45-2S, a) mainly developed vertical flexural cracks at mid-span, while some diagonal cracks exhibited near supports in addition to flexural vertical cracks. The inclined cracks in specimens with more retrofitting bars (BR45-2B1S, a) show greater resistance to brittle failure.

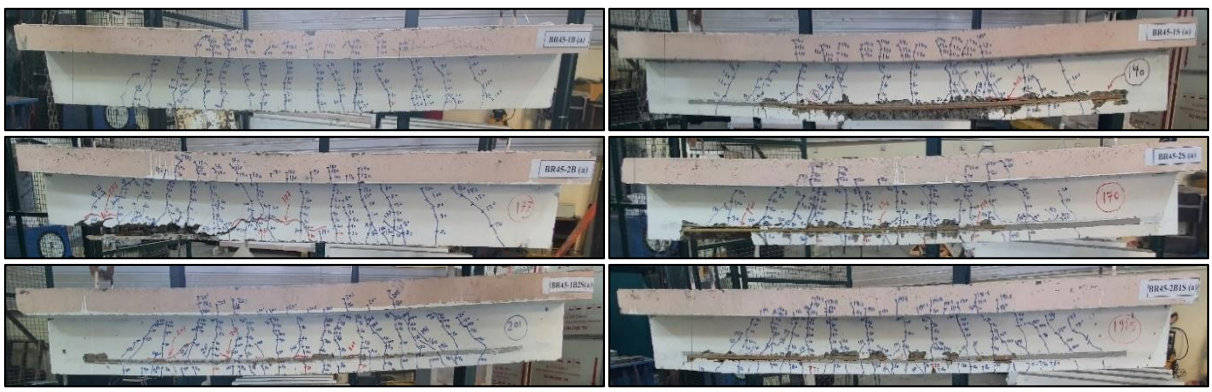

Fig.7. Cracks pattern of group one

The' cracking pattern in group two Fig. 8 shows a better uniform and extensive cracking distribution than in group one, where the vertical flexural cracks are deeper and more evenly distributed in beams such as (BR85-1B, a) and (BR85-1S, a). In (BR85-2B, a) and (BR85-2S, a), the inclined cracks propagated toward supports, and their interaction with vertical flexural cracks is denoted balanced crack control. Beams like (BR85-2B1S, a) showed extensive diagonal cracking near supports, reflecting high ductility and energy absorption capacity. Hence, the superior cracking pattern in group two highlighted the effectiveness of enhanced retrofitting techniques in achieving improved crack control and structural efficiency.

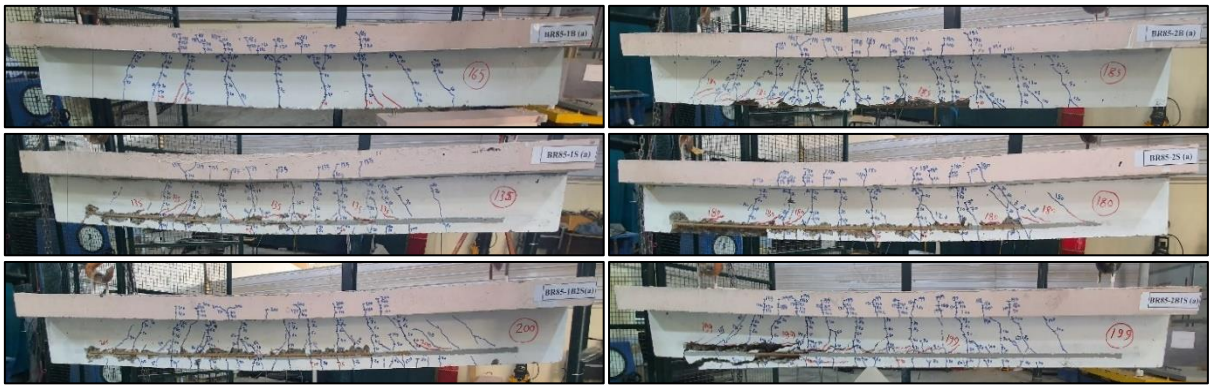

Fig. 8. Cracks pattern of group two

4. PARAMETRIC STUDY

4.1. Number of NSM-GFRP bars effect

The number of GFRP bars used in this research varied between one, two, and three, and this variety had an effect that will be explored as follows:

The comparison of the beam equipped with one bar (BR45-1B, a) and the beam retrofitted with two bars (BR45-2B, a) revealed no influence (0%) in terms of cracking load, while a substantial impact was exhibited (150% increment) with the beam of three bars (BR45-2B1S, a). For cracking deflection, the effect was very slight (7.7% decrement) when using two bars, then jumped to (81.5% increment) for the beams with three bars. Furthermore, the ultimate load-bearing capacity improved with the number of bars increasing; it recorded an 18.8% increment with the two-bar beam and a 28.9% increment with the three-bar beam. At the same time, the ultimate deflection demonstrated a general reduction with the increase of bar numbers (9.8% decrement) for the beam with two bars and (13.7% decrement) for the beam with three bars. While the assessment of the test results for the beam (BR85-1B, a) and (BR85-2B, a) showed no influence (0%) on the cracking load as well; nevertheless, an enhancement of 50% was noted in (BR85-2B1S, a). The effect on cracking deflection was around a 10.5% increase when using two bars, which escalated to 52.6% for a beam that included three bars. The maximum load-bearing capacity generally improved by increasing the number of bars, where a 12.1%

enhancement was demonstrated in the beam with two bars, and a 20.6% increase in the three bars beam. Meanwhile, the maximum mid-span deflection demonstrated an overall decrease corresponding to the increase in the number of bars, reflecting a 20.8% lower for the beam with two bars and a 14.5% decrease for the beam with three bars.

The test findings of (BR45-1S, a) against (BR45-2S, a) indicated no effect on the cracking load, whereas a major improvement (100% increase) was seen in the beam (BR45-1B2S, a). The impact on cracking deflection was about an 18.5% reduction when utilizing two bars, which subsequently escalated to 92.3% for beams with three bars. The ultimate load-bearing capacity was enhanced with the increase in bars, exhibiting an approximate 21.4% increase with the two-bar beam and a 43.6% increase with the three-bar beam. Simultaneously, the final deflection displayed a general decline with the increment of bars, showing a 1.4% reduction for the beam with two bars and a 17.5% reduction for the beam with three bars. Similarly, the evaluation of the test outcomes for the beam (BR85-1S, a) and (BR85-2S, a) showed no effect (0%) on cracking load; likewise, nonetheless, an improvement (50% increase) was observed in the beam (BR85-1B2S, a). The influence on cracking deflection was minimal, with about a 9.7% decrease when employing two bars, which then rose to 16.7% for a beam with three bars. The ultimate load-bearing capacity was enhanced with the increase in bars, showing a 33.3% improvement with the two-bar beam and a 48.1% increase with the three-bar beam. Uniquely, the ultimate deflection indicated an overall increase with the increment of bars, showing a 16.1% increase for the beam with two bars and a 6% increment for the beam with three bars; this behavior might be referred to the high initial load (85% of CB's Pu) applied on the beam, which led to a higher number of deep cracks that made the beam weak. Fig. 9 shows the load-deflection curves compared depending on the number of bars per beam for both groups, where all curves started from the point of average released deflections for each group before retrofitting for more accuracy.

4.2. Location effect of NSM-GFRP bars

Bars' placement location at the specimen's bottom or the lower part of the side(s) in the tension zone is another factor that will be assessed in this study. Where analyzed the test outcomes for the compared pairs (BR45-1B, a) with (BR45-1S, a), (BR85-1B, a) with (BR85-1S, a), (BR45-2B, a) with (BR45-2S, a), (BR85-2B, a) with (BR85-2S, a), and (BR85-1B2S, a) with (BR85-2B1S, a) indicated zero effect on the cracking load except (BR45-2B1S, a) and (BR45-1B2S, a) revealed a reduction of about 20% in cracking load; however, the beam (BR45-2B1S, a) showed the highest cracking load (25 kN) among both groups' beams and, at the same time, was identically equal to the CB cracking load. The cracking deflection generally demonstrated

small values; nevertheless, the pair (BR45-1B, a) and (BR45-1S, a) had no mention effect in addition to the beams (BR85-2B, a) with (BR85-2S, a) and (BR85-2B1S, a) with (BR85-1B2S, a) being almost with close values (3.2% increment & 3.4% decrement), which can be considered as well with no influence of bars' positions variety, the specimen (BR85-1B, a) showed about (26.3%) less cracking deflection compared to (BR85-1S, a), and (BR45-2B, a) was (13.2%) higher deflection than (BR45-2S, a). In contrast, the beam (BR45-1B2S, a) had the highest cracking deflection value (1.25 mm) among both groups' beams but exhibited about a 5.9% difference compared to (BR45-2B1S, a). in addition, the ultimate load-bearing capacity of the following compared beams (BR45-1B, a) with (BR45-1S, a), (BR85-1B, a) with (BR85-1S, a), (BR45-2B, a) with (BR45-2S, a), (BR85-2B, a) with (BR85-2S, a), (BR45-2B1S, a) with (BR45-1B2S, a) and (BR85-2B1S, a) with (BR85-1B2S, a) mostly witnessed minor variations due to altering bars' locations (-6%, -18.2%, -4%, -2.7%, 4.7%, and 0.5%) respectively, regardless of the substantial improvement in ultimate capacity compared with the CB value. On top of that, the changes in the NSM-GFRP bars' positions of the same previously compared pairs demonstrated the following differences in maximum deflection (21.7%, -11.8%, 33.1%, 29.4%, 16.4%, and 9.3%), respectively; nonetheless, the bottom bar(s) were reducing the deflection compared to side(s) bars, except for the beams (BR85-1B, a) and (BR85-1B2S, a). Fig. 10 shows the load-deflection curves compared depending on the placement locations of bars for both groups, noting that the curves started from the point of average released deflections for each group before repairing.

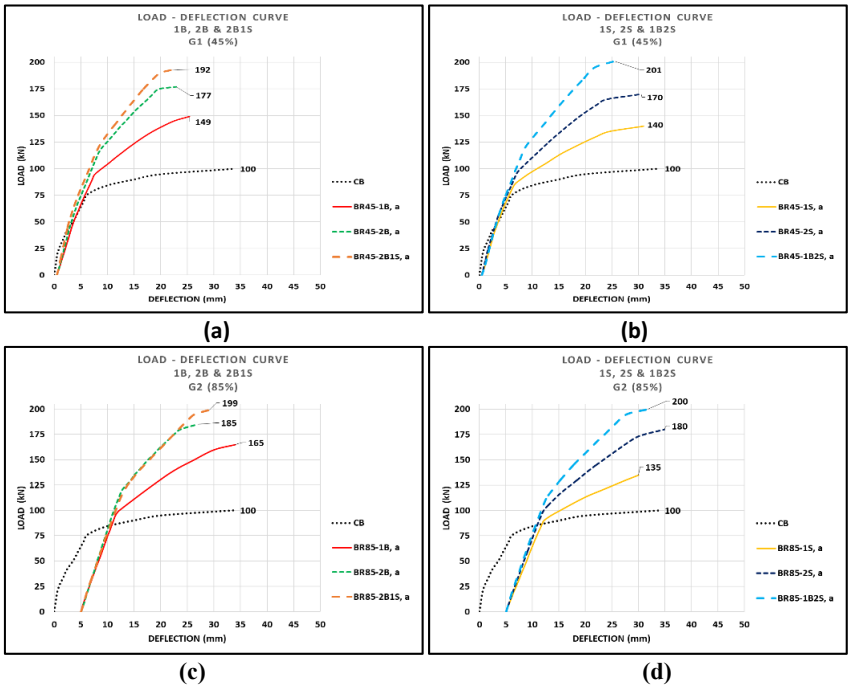

Fig. 9. Load-deflection curves comparison based on the number of bars per beam for both groups

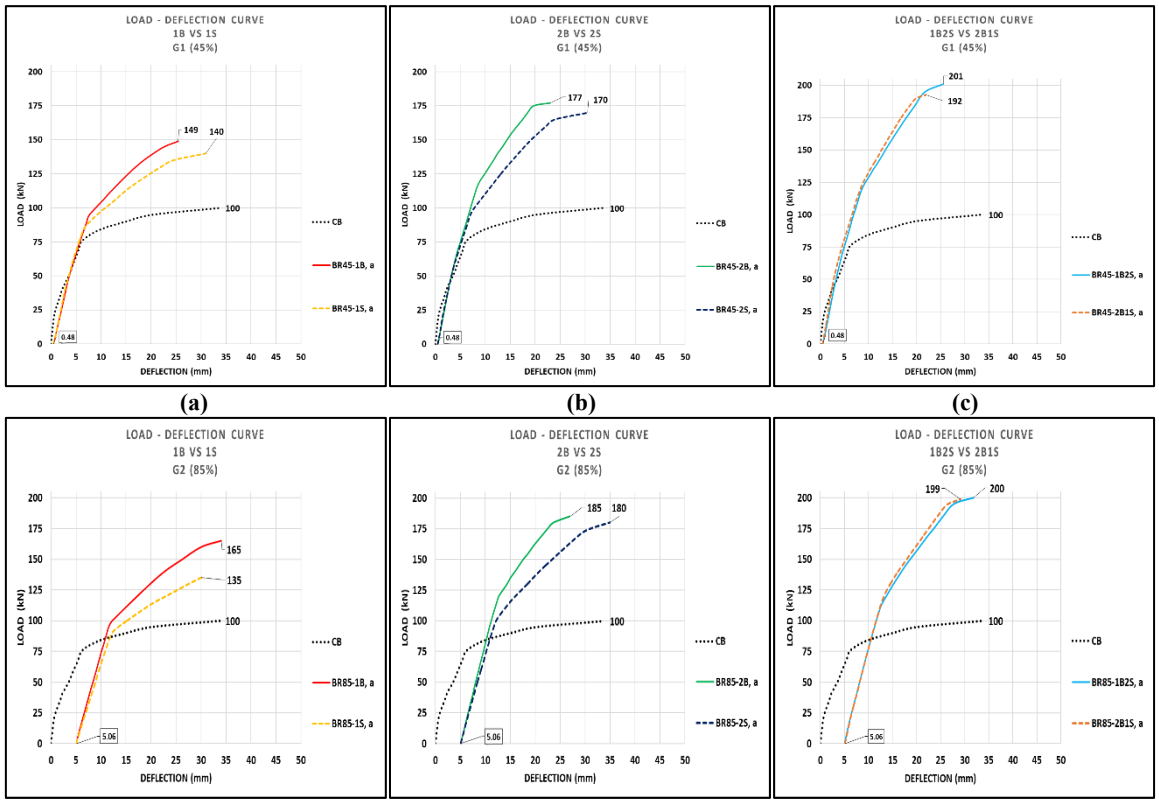

Fig. 10. Load-deflection curves comparison based on bars locations for both groups

4.3. Retrofitting type effect

The effect of retrofitting type on cracking load of the compared pairs (BR45-1B, a) and (BR85-1B, a), (BR45-1S, a) and (BR85-1S, a), (BR45-2B, a) and (BR85-2B, a), as well as (BR45-2S, a) and (BR85-2S, a) was zero percent. Whereas the pairs (BR45-1B2S, a) and (BR85-1B2S, a) along with (BR45-2B1S, a) and (BR85-2B1S, a) exhibited variations of approximately (-25% and -40%), respectively, which means the 45% of CB's Pu retrofitting type showed a positive effect in the beams with a three-bars arrangement that allowed keeping the cracking load close to or equal to the value of CB. For cracking deflection, the influence of loading level alteration of the same beams' pairs yielded the respective percentages (-12.3%, 10.8%, 5%, 22.6%, -32.8%, -26.3%). Furthermore, at 45% of CB's Pu retrofitting type, it was noticed that the two minimum cracking deflections were recorded for the beams with only two GFRP bars, while at 85% of CB's Pu, it was seen in the beams with single or double GFRP bars at the bottom only. However, the effect of retrofitting was obvious at 85% of CB's Pu, where the beams with three bars witnessed less deflection than their counterparts at 45% of CB's Pu type. Concerning the ultimate loading, the effect of loading variety on the same ordered group of pairs yielded values of 10.7%, -3.6%, 4.5%, 5.9%, -0.5%, and 3.6%, respectively; the retrofitting at 85% of CB's Pu almost had the higher improvement effect on the ultimate load. In addition, the influence on the maximum deflection of the same group of analyzed pairs was generally higher at 85% of CB's

Pu across all pairs (33.9%, -2.9%, 17.7%, 14.4%, 24.7%, and 32.7%), except for beams incorporating a single GFRP bar at the side that showed an opposite minor variation (3%) at 45% of CB's Pu. Fig. 11 shows the Load-Deflection Curves for retrofitting types.

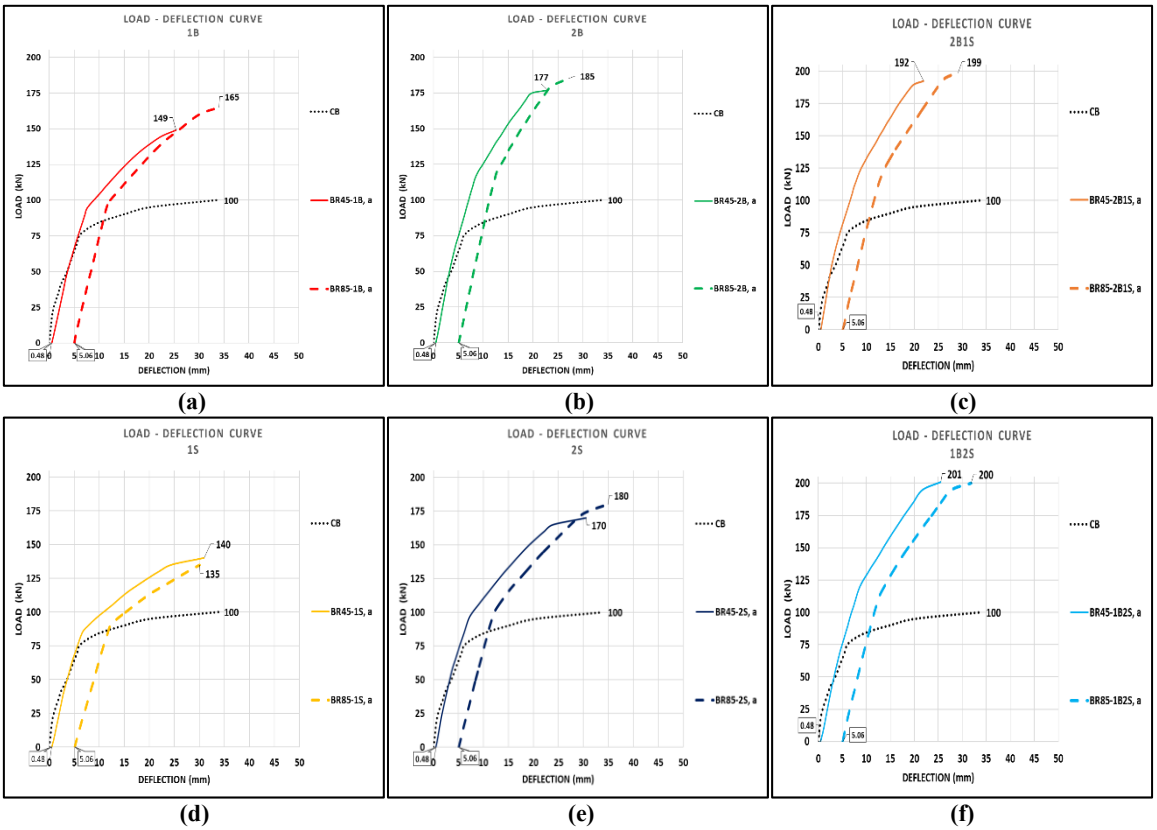

Fig. 11. Load-deflection curves comparison based on group retrofitting type.

5. CONCLUSION

1. Generally, the ultimate bearing capacities of beams retrofitted with GFRP bars witnessed a notable enhancement ranging from 35% to 101%.
2. The effects of changing bar(s) locations from (1S to 1B, 2S to 2B, and 2B1S to 1B2S) were generally enhancements for group one (6.4%, 4.1%, and 4.7%) and group two (22.2%, 2.8%, and 0.5%), respectively while the deflections of both groups were (-17%, -24.9%, 16.4%, 13.3%, -22.7%, and 9.3%).
3. The effect of increasing the bar's number on ultimate load enhancement was more noticeable in the bottom bars of group one (18.8% & 28.9%), while in group two, it was in the side(s) bars (33.3% & 48.1%). In contrast, ultimate deflections increased only in group two's side(s) bars (16.1% & 6%).
4. Toughness increments were between 11.72% and 31.96%.
5. The decrements in stiffness were between 2.36% and 47.83%, while the decreases in ductility were 55.89%-73.8%.

6. Significant improvements were recorded in cracking load between 50% and 150% when increasing the bars from one to three, while increasing the bars from one to two had no effect.
7. Deflections at the loading release case were 0.48 mm for group one and 5.06 mm for group two.

6. REFERENCES

Al Shami, A.M.H. (2022) Shear behavior of hybrid tee section concrete beams with openings and strengthened by CFRP laminates. Master's dissertation, Faculty of Engineering, University of Kufa, Iraq.

Al Thairy, H. and Youssef, A.J. (2023) 'Flexural and shear behaviour of lightweight RC beams strengthened by NSM GFRP bars', Journal of Building Pathology and Rehabilitation, 8, Article number: 31. Available at: https://doi.org/10.1007/s41024-023-00276-4.

Al-Hilfi, A.L.A. and Al-Katib, H.A.A. (2024) 'Retrofitting of hybrid concrete beams in shear using externally bonded CFRP sheets', The 5th International Conference on Civil and Environmental Engineering Technologies, AIP Conference Proceedings, 3249, pp. 020012-1–020012-18. Available at: https://doi.org/10.1063/5.0236561.

Aljebory, S.M. and Kamonna, H.H. (2025) 'Repairing of continuous one-way reinforced concrete slabs by CFRP composites', Kufa Journal of Engineering, 16(1), pp. 324–343. Available at: https://doi.org/10.30572/2018/KJE/160119.

Al-Katib, H.A.A. and AL-Turaihi, A.A.A. (2024) 'Behavior of hybrid reinforced concrete beams on flexural strength', Kufa Journal of Engineering, 15(2), pp. 27–38. Available at: https://doi.org/10.30572/2018/KJE/150203.

Al-Katib, H.A.A. and AL-Turaihi, A.A.A. (2024) 'Effect of GFRP bar length on the flexural behavior of hybrid concrete beams strengthened with NSM bars', Open Engineering. Available at: https://doi.org/10.1515/eng-2022-0538.

American Concrete Institute (2017) ACI 440.2R-17: Guide for the design and construction of externally bonded FRP systems for strengthening concrete structures. ACI Committee 440.

American Concrete Institute (2019) ACI CODE-318-19: Building code requirements for structural concrete and commentary. ACI Committee 318.

ASTM International (2024) ASTM A615/A615M-24: Standard specification for deformed and plain carbon steel bars for concrete reinforcement. West Conshohocken, PA. Available at: https://doi.org/10.1520/A0615_A0615M-24.

BenSaoud, M., Oraf, M., Gundogay, A., Yaman, S., Eren, V. and Kabas, H.T. (2024) 'An experimental study on repairing of reinforced concrete beams having damaged longitudinal bars', Applied Sciences, 14(23), Article number: 11310. Available at: https://doi.org/10.3390/app142311310.

Hosen, M.A., Alengaram, U.J., Jumaat, M.Z., Sulong, N.H.R. and Darain, K.M. (2017) 'Glass fiber reinforced polymer (GFRP) bars for enhancing the flexural performance of RC beams using side-NSM technique', Polymers, 9(5), p.180. Available at: https://doi.org/10.3390/polym9050180.

Hosen, M.A., Jumaat, M.Z., Alsubari, B., Sulong, N.H.R., Ibrahim, Z., Alengaram, U.J. and Hashim, H. (2020) 'Effect of bonding materials on the flexural improvement in RC beams strengthened with SNSM technique using GFRP bars', Journal of Building Engineering, 32, 101777. Available at: https://doi.org/10.1016/j.jobe.2020.101777.

Joudah, R.S. and Al-Katib, H.A.A. (2024) 'Flexural behavior for repairing of hybrid concrete beams by NSM-GFRP bars', The 5th International Conference on Civil and Environmental Engineering Technologies, AIP Conference Proceedings, 3249, pp. 020016-1–020016-15. Available at: https://doi.org/10.1063/5.0237250.

Kamonna, H.H. and Abd Al-Sada, D.J. (2021) 'Effect of near-surface mounted bars on the structural behavior of one-way RC slab', Kufa Journal of Engineering, 12(3), pp. 12–30. Available at: http://dx.doi.org/10.30572/2018/KJE/120302.

Marzoq, Z.H. and Borhan, T.M. (2020) 'The behaviour of hybrid reinforced concrete T beams exposed to the flexural moment', Asian Journal of Civil Engineering, 21, pp. 1005–1012. Available at: https://doi.org/10.1007/s42107-020-00257-9.

Reda, R.M., Sharaky, I.A., Ghanem, M., Seleem, M.H. and Sallam, H.E.M. (2016) 'Flexural behavior of RC beams strengthened by NSM GFRP bars having different end conditions', Composite Structures, 147, pp. 131–142. Available at: https://doi.org/10.1016/j.compstruct.2016.03.018.

Sharaky, I.A., Torres, L., Comas, J. and Barris, C. (2014) 'Flexural response of reinforced concrete (RC) beams strengthened with near surface mounted (NSM) fibre reinforced polymer (FRP) bars', Composite Structures, 109, pp. 8–22. Available at: https://doi.org/10.1016/j.compstruct.2013.10.051.

Tahmouresi, B., Momeninejad, K. and Mohseni, E.E. (2022) 'Flexural response of FRP strengthened lightweight RC beams: hybrid bond efficiency of L-shape ribbed bars and NSM technique', Archives of Civil and Mechanical Engineering, 22, Article number: 95. Available at: https://doi.org/10.1007/s43452-022-00410-y.

Tang, W.C., Balendran, R.V., Nadeem, A. and Leung, H.Y. (2006) 'Flexural strengthening of reinforced lightweight polystyrene aggregate concrete beams with near-surface mounted GFRP bars', Building and Environment, 41(10), pp. 1381–1393. Available at: https://doi.org/10.1016/j.buildenv.2005.05.029.